Plasmon excitation in beryllium: inelastic x-ray scattering experiments and first-principles calculations

2007 J. Phys.: Condens. Matter 19 046207

(http://iopscience.iop.org/0953-8984/19/4/046207)

INSTITUTE OF PHYSICS PUBLISHING JOURNAL OF PHYSICS: CONDENSED MATTER

J. Phys.: Condens. Matter **19** (2007) 046207 (11pp) doi:10.1088/0953-8984/19/4/046207

Plasmon excitation in beryllium: inelastic x-ray scattering experiments and first-principles calculations

G Tirao[1], G Stutz[1], V M Silkin[2], E V Chulkov[3] and C Cusatis[4]

[1] Fa.M.A.F., Universidad Nacional de Córdoba, 5000 Córdoba, Argentina
[2] Donostia International Physics Center (DIPC), Paseo de Manuel Lardizabal, 4, 20018 San Sebastián, Basque Country, Spain
[3] Departamento de Física de Materiales and Centro Mixto CSIC-UPV/EHU, Facultad de Ciencias Químicas, Universidad del País Vasco, Apartado 1072, 20080 San Sebastián, Basque Country, Spain
[4] Departamento, de Física, Universidade Federal do Paraná, 81531 Curitiba, PR, Brazil

E-mail: stutz@famaf.unc.edu.ar and waxslavs@sc.ehu.es (V M Silkin)

Received 5 September 2006
Published 12 January 2007
Online at stacks.iop.org/JPhysCM/19/046207

Abstract

An experimental and theoretical study of collective electronic excitations in Be is presented. The plasmon energy and linewidth were measured by means of inelastic x-ray scattering spectroscopy. Measurements were performed on a polycrystalline sample and in a broad range of momentum transfers within the plasmon excitation regime. Theoretical plasmon dispersion and its linewidth in the whole Brillouin zone were derived from *ab initio* evaluations of the electron density response function. The calculations were performed with full inclusion of the electron band structure within the random-phase approximation. Good agreement of experimental plasmon energy and linewidth dispersions with direction-averaged theoretical results in all investigated q-range is obtained. We conclude that, in Be, the band structure effects alone can account for the observed finite plasmon lifetime at $q = 0$, as well as for the linewidth dispersion in the long-wavelength domain.

1. Introduction

Synchrotron-radiation-based inelastic x-ray scattering spectroscopy (IXSS) as a probe of bulk excited-state properties of electron systems in condensed matter has become a well-established technique in the last two decades [1]. Besides having been applied to extensive studies of the dynamic structure factor of valence electrons in the region of intermediate momentum transfer, dominated by single-particle excitations (see the review by Schülke [1] and references therein), IXSS has also been applied successfully to investigate collective electronic excitations at lower momentum transfers in a large variety of materials [2–8]. Although the latter field is the domain of the electron energy-loss spectroscopy (EELS) [9], the application of IXSS as a unique

experimental tool for studying plasmon excitations in liquid metals [3–7] is worth mentioning. The inelastic x-ray scattering cross section is proportional to the imaginary part of the inverse dielectric function (the so-called energy-loss function) [10], which plays a fundamental role in the theoretical study of elementary excitations in many-particle systems. Thus, IXSS experiments give insight into understanding the frequency and wavevector dependence of the response function of a correlated electron system.

Early experiments on inelastic x-ray scattering by plasmon excitation in Be were performed using conventional x-ray sources [11–14]. Those measurements suffered from limited energy resolution, due to the finite natural linewidth of the characteristic x-rays, from contamination of the energy-loss spectrum by bremsstrahlung, giving rise to a very low signal-to-background ratio, or from overlapping of energy-loss spectra, due to the K_α-doublet structure. Furthermore, the potentiality of the near back-diffraction for energy analysis with high resolution had not been exploited up to the time of those early experimental works. The first high-resolution IXSS measurements on Be using monocromated synchrotron x-rays were performed by Schülke *et al* [15]. That study focused on investigating the dynamic structure factor of valence electrons in the region of intermediate momentum transfer.

It is well known that the measured plasmon dispersion relation of simple metals deviates from predictions of the random-phase approximation (RPA) for a homogeneous, non-interacting electron gas. Non-RPA effects arising from the exchange and Coulomb correlations were introduced through a static local-field correction by different theoretical approaches (see, e.g., the early reviews by Ichimaru [16] and Singwi and Tosi [17]). This correction improved the RPA predictions lowering the dispersion of the plasmon energy, but it was not sufficient to achieve a good quantitative agreement with experimental results [3, 18, 19]. Even a dynamical local-field correction [20] was also unable to account for deviations between the theoretical and experimental plasmon dispersion coefficients of alkali metals [19]. From first-principles evaluation of the dynamical density-response function of Al and Na, with full inclusion of the effects of the crystal structure, Quong and Eguiluz [21] showed that the observed deviations of the plasmon dispersion from the RPA prediction for a homogeneous electron gas are attributable mainly to band-structure effects. In the case of Be, *ab initio* calculations of the dynamic response of valence electrons were carried out by Maddocks *et al* [22] in the regime of particle–hole-pair excitations. They established that band-structure effects are responsible for all the fine structure experimentally observed by Schülke *et al* [15] in the dynamic structure factor of Be. In the region of low momentum transfer, plasmon dispersion curves for Be were recently derived by Silkin *et al* [23] from *ab initio* calculations of the inverse dielectric matrix with full inclusion of band-structure effects. The incorporation of these effects was shown to be essential in order to improve significantly the agreement between the calculated and measured electron inelastic mean free paths in Be. Concerning the effects of the band structure on the wavevector dependence of the plasmon linewidth, it has been demonstrated by Sturm [24], including the crystal potential in a perturbative way, that interband transitions may make the major contribution in some simple metals like Al and Li, besides being the decay mechanism responsible for the non-vanishing half-width at zero momentum transfer. The peculiar behaviour of the plasmon linewidth in Li was subsequently confirmed to be due to the band structure from *ab initio* calculations, which have taken fully into account the crystal potential [25]. Another illustration of the important role played by interband transitions in plasmon damping processes is the explanation of the 'anomalous' dispersion of the plasmon width in K by Ku and Eguiluz [26] from *ab initio* calculations of the electron density response within the framework of time-dependent density-functional theory. These authors found that the key decay channel in K is the excitation of particle–hole pairs involving empty d-states. *Ab initio* band-structure calculations have recently been used by Keast [27] to predict the low-loss

EELS spectra, including the plasmon energy and width, for many elements and some simple compounds, but only at zero momentum transfer. For Be, to our knowledge, calculations of the plasmon linewidth and its wavevector dependence, including band structure effects, have not been reported so far.

It is the purpose of this work to investigate collective excitations in Be both experimentally, with high energy and momentum resolution, and theoretically, including full band-structure effects. Energy-loss spectra were measured by means of inelastic x-ray scattering spectroscopy and for momentum transfers covering the whole range of the plasmon excitation domain ($q < q_c, q_c$ being the critical plasmon wavevector). The theoretical wavevector-dependent plasmon energy and linewidth are derived from high-precision *ab initio* evaluations of the electron response function, which includes the full effects of the crystal lattice.

2. Calculation details

Observables such as the inelastic scattering cross section for x-rays and fast electrons are related to the dynamical density-response function $\chi(\mathbf{r}, \mathbf{r}', \omega)$ of an interacting electron system, which, in general, is a non-local energy-dependent function. Within the linear-response theory, it relates to the electron density, $n^{\mathrm{ind}}(\mathbf{r}, \omega)$, induced in the system due to an external perturbation potential, $V^{\mathrm{ext}}(\mathbf{r}, \omega)$, through the equation

$$n^{\mathrm{ind}}(\mathbf{r}, \omega) = \int \mathrm{d}\mathbf{r}' \chi(\mathbf{r}, \mathbf{r}', \omega) V^{\mathrm{ext}}(\mathbf{r}', \omega) \tag{1}$$

and does not depend on the exact form of $V^{\mathrm{ext}}(\mathbf{r}, \omega)$, being a characteristic of the system. In the framework of time-dependent density-functional theory [28, 29], $\chi(\mathbf{r}, \mathbf{r}', \omega)$ obeys the integral equation

$$\begin{aligned}\chi(\mathbf{r}, \mathbf{r}', \omega) = {} & \chi^0(\mathbf{r}, \mathbf{r}', \omega) \\ & + \int \mathrm{d}\mathbf{r}_1 \int \mathrm{d}\mathbf{r}_2 \chi^0(\mathbf{r}, \mathbf{r}_1, \omega)[\upsilon(\mathbf{r}_1 - \mathbf{r}_2) + K^{\mathrm{xc}}(\mathbf{r}_1, \mathbf{r}_2, \omega)]\chi(\mathbf{r}_2, \mathbf{r}', \omega),\end{aligned} \tag{2}$$

where $\chi^0(\mathbf{r}, \mathbf{r}', \omega)$ is the density-response function for a non-interacting electron system, $\upsilon(\mathbf{r} - \mathbf{r}')$ is the bare Coulomb potential, and $K^{\mathrm{xc}}(\mathbf{r}, \mathbf{r}', \omega)$ accounts for dynamical exchange–correlation effects. For a periodic crystal, one can expand all these quantities in Fourier series. Then, the integral equation (2) transforms into a matrix equation

$$\begin{aligned}\chi_{\mathbf{G},\mathbf{G}'}(\mathbf{q}, \omega) = {} & \chi^0_{\mathbf{G}}, \mathbf{G}'(\mathbf{q}, \omega) \\ & + \sum_{\mathbf{G}''} \sum_{\mathbf{G}'''} \chi^0_{\mathbf{G},\mathbf{G}''}(\mathbf{q}, \omega)[\upsilon_{\mathbf{G}''}(\mathbf{q})\delta_{\mathbf{G}'',\mathbf{G}'''} + K^{\mathrm{xc}}_{\mathbf{G}'',\mathbf{G}'''}(\mathbf{q}, \omega)]\chi_{\mathbf{G}''',\mathbf{G}'}(\mathbf{q}, \omega).\end{aligned} \tag{3}$$

Here, $\mathbf{G}$ is a vector of the reciprocal lattice, and the Fourier coefficients $\chi^0_{\mathbf{G},\mathbf{G}'}(\mathbf{q}, \omega)$ have the form

$$\begin{aligned}\chi^0_{\mathbf{G},\mathbf{G}'}(\mathbf{q}, \omega) = {} & \frac{2}{\Omega} \sum_{\mathbf{k}}^{BZ} \sum_{n,n'} \frac{f_{n\mathbf{k}} - f_{n'\mathbf{k}+\mathbf{q}}}{\varepsilon_{n\mathbf{k}} - \varepsilon_{n'\mathbf{k}+\mathbf{q}} + (\omega + \mathrm{i}\eta)} \\ & \times \langle \psi_{n\mathbf{k}} | \mathrm{e}^{-\mathrm{i}(\mathbf{q}+\mathbf{G})\cdot\mathbf{r}} | \psi_{n'\mathbf{k}+\mathbf{q}} \rangle \langle \psi_{n'\mathbf{k}+\mathbf{q}} | \mathrm{e}^{\mathrm{i}(\mathbf{q}+\mathbf{G}')\cdot\mathbf{r}} | \psi_{n\mathbf{k}} \rangle,\end{aligned} \tag{4}$$

where Ω is the normalization volume, the factor 2 accounts for spin, the sums over n and n' run over the band structure for wavevectors in the first Brillouin zone (BZ), $f_{n\mathbf{k}}$ is the Fermi distribution function, $\varepsilon_{n\mathbf{k}}$ and $\psi_{n\mathbf{k}}(\mathbf{r})$ are Bloch eigenvalues and eigenfunctions of the Kohn–Sham Hamiltonian, and η is a positive infinitesimal. Equation (4) is a key ingredient of our calculations. In practice, the matrix $\chi^0_{\mathbf{G},\mathbf{G}'}(\mathbf{q}, \omega)$ is evaluated by introducing some small value of η or performing calculations at imaginary [26] or complex [22] frequencies ω with subsequent analytical continuation to the real axis. Here we employ another approach based on

the evaluation of the spectral function matrix $S_{\mathbf{G},\mathbf{G}'}(\mathbf{q},\omega)$ [30, 31] with subsequent evaluation of the imaginary part of $\chi^0_{\mathbf{G},\mathbf{G}'}(\mathbf{q},\omega)$ using the relation

$$S_{\mathbf{G},\mathbf{G}'}(\mathbf{q},\omega) = \frac{1}{\pi}\,\mathrm{Im}\left[\chi^0_{\mathbf{G},\mathbf{G}'}(\mathbf{q},\omega)\right]\mathrm{sgn}(\omega). \tag{5}$$

Once the imaginary part of $\chi^0_{\mathbf{G},\mathbf{G}'}(\mathbf{q},\omega)$ is evaluated, its real part is obtained by performing a Hilbert transform. Information on the energy and lifetime of the Be bulk plasmon for a given $\mathbf{q}$ has been obtained from the evaluation of the dynamical-structure factor

$$S(\mathbf{q},\omega) = -\frac{2\hbar\Omega}{\upsilon_0(\mathbf{q})}\,\mathrm{Im}\left[\epsilon^{-1}_{\mathbf{G}=0,\mathbf{G}'=0}(\mathbf{q},\omega)\right], \tag{6}$$

where $\mathrm{Im}\left[\epsilon^{-1}_{\mathbf{G}=0,\mathbf{G}'=0}(\mathbf{q},\omega)\right]$ is the energy-loss function related to the response function $\chi_{\mathbf{G},\mathbf{G}'}(\mathbf{q},\omega)$ through

$$\epsilon^{-1}_{\mathbf{G},\mathbf{G}'}(\mathbf{q},\omega) = \delta_{\mathbf{G},\mathbf{G}'} + \upsilon_{\mathbf{G}}(\mathbf{q})\chi_{\mathbf{G},\mathbf{G}'}(\mathbf{q},\omega). \tag{7}$$

The calculations have been performed for a hexagonal closed-packed Be lattice with experimental lattice parameters $a = 2.285$ Å and $c = 3.585$ Å [32]. The one-particle energies $\varepsilon_{n\mathbf{k}}$ and wavefunctions $\psi_{n\mathbf{k}}(\mathbf{r})$ were evaluated as a self-consistent solution of the Kohn–Sham equations with the use of an exchange–correlation potential in the form of [33]. In our calculations the electron–ion interaction is described by a non-local, norm-conserving ionic pseudo-potential [34, 35], and $\psi_{n\mathbf{k}}(\mathbf{r})$ were expanded in a plane-wave basis up to a kinetic-energy cutoff of 24 Ryd. Twenty reciprocal vectors, $\mathbf{G}$, were included in the Fourier expansions of χ^0, χ, and ϵ. In equation (4) the sum in $\mathbf{k}$ includes a $72 \times 72 \times 24$ sampling, which corresponds to 124 416 points in the BZ. The sum over n and n' included all energy bands up to an energy of 50 eV above the Fermi level. We solve equation (3) using the random-phase approximation, taking $K^{\mathrm{xc}} = 0$. As shown by Maddocks *et al* [22], this is a fairly good approximation for Be due to its high valence electron density (for Be $r_s = 1.866$). Note that, in the present calculations, the local crystal fields are incorporated in the evaluation of $S(\mathbf{q},\omega)$ through the inclusion of non-diagonal matrix elements in $\chi^0_{\mathbf{G},\mathbf{G}'}(\mathbf{q},\omega)$.

The frequency $\omega_p(\mathbf{q})$ and the linewidth $\Delta_p(\mathbf{q})$ of the plasmon are obtained from $\mathrm{Im}\left[\epsilon^{-1}_{\mathbf{G}=0,\mathbf{G}'=0}(\mathbf{q},\omega)\right]$ for a given wavevector $\mathbf{q}$. For comparison with experimental dispersions deduced from measurements on polycrystalline samples, we have performed direction-averaged calculations of the dynamical structure factor. For this, we have calculated $S(\mathbf{q},\omega)$ for the same set of wavevectors $\mathbf{q}$ that was used for $\mathbf{k}$ in the evaluation of $\chi_{\mathbf{G},\mathbf{G}'}(\mathbf{q})$ in equation (4). Finally, we calculate $S_{\mathrm{av}}(q,\omega)$ as

$$S_{\mathrm{av}}(q,\omega) = \frac{\sum^{\mathrm{ZB}}_{\mathbf{q}'} S(\mathbf{q}',\omega)\mathrm{e}^{-(q-|\mathbf{q}'|)^2/\Delta^2}}{\sum^{\mathrm{ZB}}_{\mathbf{q}'} \mathrm{e}^{-(q-|\mathbf{q}'|)^2/\Delta^2}}. \tag{8}$$

The final direction-averaged $\omega_p(q)$ and $\Delta_p(q)$ are obtained from the fitting of $S_{\mathrm{av}}(q,\omega)$ with one Lorentzian. We have proven that $\omega_p(q)$ and $\Delta_p(q)$ change less than 0.1 eV for Δ in the range 0.01–0.03 au. The extrapolated $\omega_p(q \to 0) = 19.05$ eV and $\Delta_p(q \to 0) = 5.15$ eV for small q are in excellent agreement with the values $\omega_p = 19.4$ eV and $\Delta_p = 5.1$ eV, recently calculated with the full-potential linearized augmented plane-wave method [27].

3. Experimental details and data processing

Inelastic x-ray scattering experiments were carried out on the D12A-XRD1 beamline at the LNLS (National Synchrotron Light Laboratory, Brazil). The whole experimental setup is described in detail in [36]. Briefly, it consists of a sagittally focusing double-crystal Si(111)

monochromator in a non-dispersive setting and a high-resolution Rowland-type spectrometer based on a spherically focusing nearly-backdiffracting Si(333) analyser. An x-ray mirror placed upstream of the monochromator provided vertical focalization. The analyser was positioned at a fixed Bragg angle of 89.2°, and thus tuned to analyse radiation of 5.93 keV. Energy-loss scans were accomplished by scanning the energy of the incident photon beam. Si pin-diode detectors were used to monitor the flux of the incident beam and to record the signal of inelastically scattered photons. The whole spectrometer was installed in a chamber evacuated to 5×10^{-2} mbar to avoid loss of intensity due to air absorption and to reduce the background arising from air scattering. In order to probe collective electronic excitations in Be, measurements were performed at low momentum transfer, for magnitudes ranging from 0.11 to 0.61 au (scattering angles from 4° to 22°, respectively). The covered range is well below the critical wavevector for Be of $q_c = 0.73$ au.[5] Measurements were performed on a 2.2 mm-thick polycrystalline sample using symmetrical transmission geometry. This thickness matches the mean free path of the incident photons in Be, which allows the scattering power to be maximized. The beam dimensions at the sample position were 2.5 mm (h)× 1.6 mm (v). The angular acceptance of the analyser was limited by means of annular diaphragms [36] to improve the momentum resolution without diminishing to a large extent the collected solid angle. The angular aperture of the diaphragms was 1.1°, giving rise to a full transferred-momentum resolution of 0.03 au, which is nearly independent of the scattering angle within the measured range. The analyser collected scattered radiation in a solid angle varying from 4.7 msr at 4° to 4.2 msr at 22°. The total energy resolution of the spectrometer was 1.08±0.07 eV, which was determined from the mean value of the widths (FWHM) of the elastic peaks. Throughout the measurements, the stability of the elastic line was better than ±0.15 eV. The counting rate at the plasmon peak at 100 mA ring current increased from 4 counts s^{-1} at the lowest momentum transfer to 34 counts s^{-1} at the highest momentum transfer; the peak signal-to-background ratio was better than 5 and 100, respectively. The background intensity is related to the low-energy-loss side of the elastic peak. Depending on the scattering angle, between about 10^3 and 2.5×10^3 counts were collected in a single measuring point at the maximum of the inelastic peak.

In figure 1 experimental energy-loss spectra of Be measured for different q values are presented. A constant background, as determined from the low-energy-loss side of the elastic peak, was subtracted. The scattered intensity is normalized to the signal of the monitor, placed between the monochromator and the scattering sample. The data therefore do not need to be corrected for the weak energy dependence of the monochromator reflectivity. Since the largest variation of the incident energy when making energy-loss scans is only ∼40 eV, corrections due to the weak energy dependence of the scattering cross section can be neglected. The influence of multiple scattering processes on the energy-loss spectra is negligible in IXSS, as evidenced experimentally in [15] and [37], and confirmed later by means of Monte Carlo studies [38]. In contrast, in EELS, multiple events can distort the plasmon peak in Be appreciably for q-values approaching q_c [39]. The inelastic peaks were fitted with Voigt functions, where the half-width of the Gaussian function, which should simulate the instrumental response, was set to be the experimental energy resolution. The fitting procedure provides the peak position and the half-width of the Lorentzian part of the Voigt function as fitting paramenters, from which the bulk plasmon energy and linewidth, respectively, can be obtained directly.

[5] This value corresponds to the free-electron-gas model and is obtained by solving the equation $\omega(q) = q^2/2m + qk_F/m$ numerically, the right-hand side being the dispersion of the upper bound of the excitation continuum. The plasmon dispersion curve $\omega(q)$ is obtained from the numerical solution of $\epsilon_L(q, \omega(q)) = 0$, where ϵ_L is the Lindhard dielectric function [10]. The usual approximate expression $q_c \approx \omega_0/v_F$ (where ω_0 is the plasmon energy at zero momentum transfer and v_F is the Fermi velocity) provides a somewhat smaller value of $q_c \approx 0.66$ au.

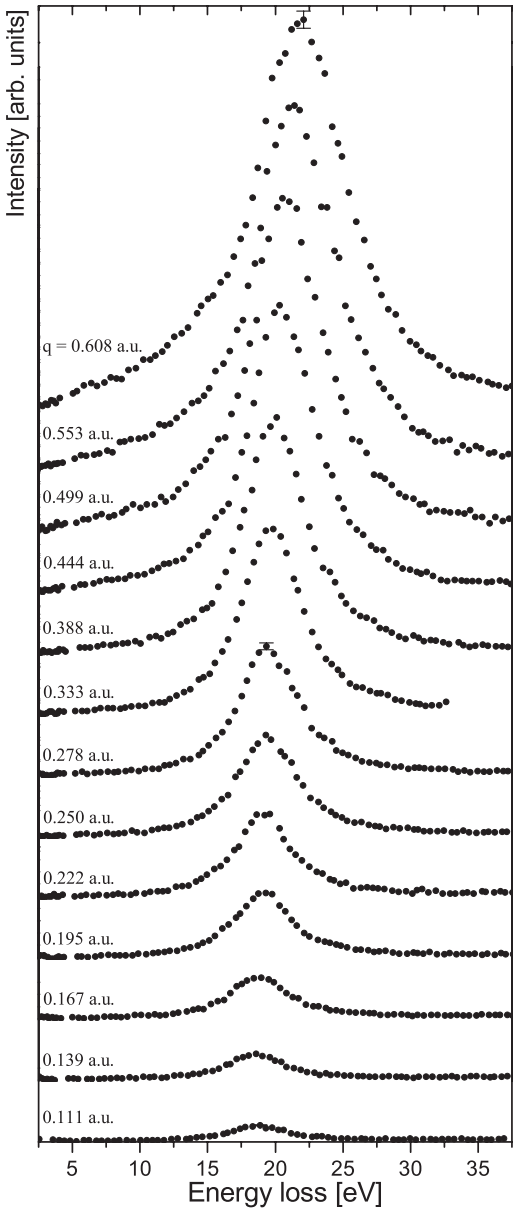

Figure 1. Experimental x-ray energy-loss spectra of polycrystalline beryllium as a function of the transferred energy for different magnitudes of momentum transfer. Error bars due to the counting statistic are shown. The spectra are displaced vertically for clarity. Elastic lines are not shown in the spectra.

4. Results and discussion

The experimental energy position of the plasmon peak as a function of momentum transfer, along with present theoretical results, are shown in figure 2. In addition to the direction-averaged curve, dispersions along some high-symmetry directions, namely parallel to the *c*-

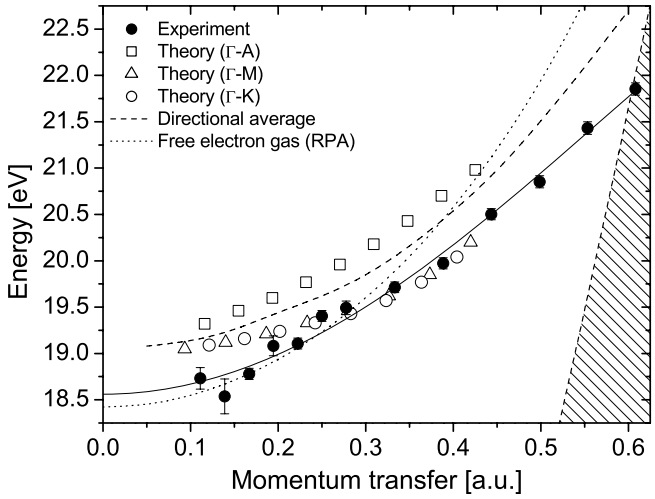

Figure 2. Plasmon energy dispersion for Be. Present measurements (filled circles) and calculations (direction-averaged (dashed), Γ–A direction (open squares), Γ–M direction (open triangles) and Γ–K direction (open circles)) are shown. The dotted line is the RPA result for a free electron gas. The shaded region denotes the continuum of particle–hole excitations. The RPA curve intersects the excitation continuum at $q_c = 0.73$ au. The solid line is the fit to the experimental data with a function of the form $\omega(q) = a + bq^2 + cq^4$.

axis (Γ–A direction) and on the hexagonal plane (Γ–M and Γ–K directions) are also shown. Theoretical directional dispersions and linewidths are presented only in the q-range where a single plasmon peak is well defined in the corresponding directional energy-loss functions. At higher momentum transfer, a double-peak structure begins to evolve and the plasmon peak becomes strongly distorted. For the sake of comparison, the plasmon dispersion for the jellium model within the RPA is included in the same figure. This curve is obtained by numerically solving $\epsilon_L(q, \omega(q)) = 0$, thus showing the exact q-dependence of the plasmon energy for the jellium model. Unlike the case of other simple metals such as Li, Na and Al, the free electron gas (FEG) model in the RPA predicts for Be a plasmon dispersion not so far from the experiment in the region of very low q-values ($q < 0.3$ au), as can be seen in figure 2. At larger momentum transfers, the FEG plasmon dispersion deviates systematically from the experiment to higher energy values as q approaches the excitation continuum. At $q \simeq 0.6$ au the deviation is as large as 10%. It is a general trend of the plasmon dispersion for an FEG to increase more rapidly with q than is observed experimentally [18, 19]. The theoretical dispersion in the Γ–A direction is systematically higher than in the hexagonal plane, where the dispersion is practically isotropic in the q-range shown. The calculated direction-averaged curve lies slightly above the experimental one, displaced by ∼0.5 eV. To obtain the plasmon energy at zero momentum transfer, a biquadratic function such as the one suggested by Sprösser-Prou *et al* [18] was fitted to the experimental points in all the measured q-range. The extrapolation of the fitted function to $q = 0$ gives a value of 18.6 ± 0.1 eV, which is in very good agreement with the EELS value of 18.7 eV [40]. These measured values are very close to the extrapolated theoretical value of 19.05 eV. In the early, medium-resolution x-ray study of Eisenberger *et al* [14] a somewhat lower value of the plasmon energy at $q = 0$ (18.35 ± 0.35 eV) was measured, in rather good accord with the present experimental value if the experimental errors are considered. The FEG plasmon energy at the electron density of Be is 18.4 eV. In Be, lattice effects shift the FEG value at $q = 0$ upwards, in contrast to Al and Na [21], whereas at large wavevectors the FEG energy is lowered by the effects of the crystal. It is known

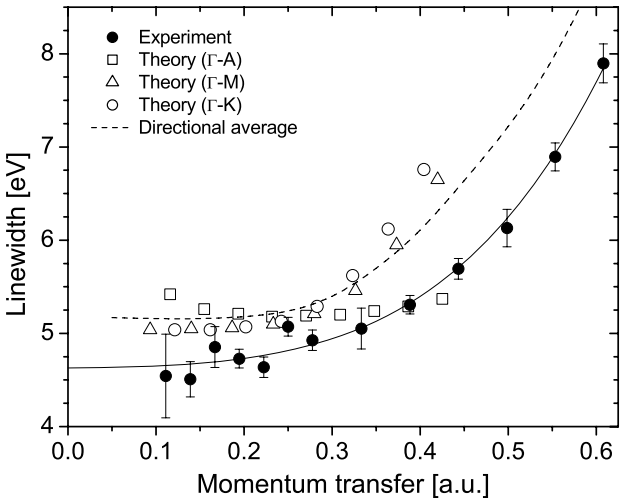

Figure 3. Plasmon linewidth dispersion for Be. Present measurements (filled circles) and calculations (direction-averaged (dashed), Γ–A direction (open squares), Γ–M direction (open triangles) and Γ–K direction (open circles)) are shown. The values correspond to the FWHM of the peaks. The solid line is the fit to the experimental data with a function of the form $\Delta(q) = a + bq^2 + cq^4$.

that if the plasmon energy is far below the core excitation energies, as in the case of Be, the contribution of the core polarization to the dielectric function causes a small red shift of the plasmon energy [41, 42]. The relative energy shift can be estimated from a simple model [42]: $\Delta\omega/\omega \simeq -\mathrm{Re}\,\Delta\epsilon_{\mathrm{core}}/2$, which is valid provided that $\Delta\epsilon_{\mathrm{core}} \ll 1$. The core contribution to the dielectric function can be evaluated using $\Delta\epsilon_{\mathrm{core}} \simeq 4\pi n_i \alpha$ [41], where n_i is the density of the ions and α is the core polarizability. In the energy-loss range in which we are interested, α can be replaced by a static polarizability. Using the free ion polarizability calculated in [43], one obtains a shift of the plasmon energy at $q = 0$ of only $\Delta\omega \simeq -0.12$ eV. Though this correction brings the calculated energy closer to the measured energy, core polarization effects in Be seem to be unable to account for the whole difference in the plasmon energy at $q = 0$. The remaining difference (<2%) could be attributed to uncertainties in the determination of the experimental plasmon energies and to numerical uncertainties in the calculations. Effects beyond RPA could also be responsible for small discrepancies in the q-dependence of the dispersion [21]. Nevertheless, an overall good agreement between theory and experiment can be concluded. This shows the importance of including lattice effects in the calculations in order to reproduce the observed dispersion quantitatively well, as demonstrated in the case of Al [21].

Regarding the plasmon linewidth, the experimental data are displayed in figure 3 as a function of the momentum transfer. The measured half-width shows a positive dispersion, as in most simple metals, and a finite extrapolated value to $q = 0$ of 4.6 ± 0.1 eV, which is in good agreement with the EELS value of 4.8 eV [40]. Results from present calculations are also shown in figure 3. A marked anisotropy, depending on whether $\mathbf{q}$ is parallel or perpendicular to the c-axis, is clearly seen. Whereas in the hexagonal plane the curves disperse positively, exhibiting a slight anisotropy for $q > 0.3$ au, along the c-axis the calculated linewidth shows a negative, weak dispersion at low momentum transfer, turning to positive at $q \sim 0.3$ au. The observed behaviour for $\mathbf{q} \parallel c$-axis can be traced back to the reduction of the phase space available for interband transitions as q increases, as proposed by other authors to explain the negative dispersion in Li [24, 25, 48]. The plasmon linewidth extracted

from the direction-averaged energy-loss function shows a positive net dispersion and lies very close to the experimental curve. The difference between them is only 0.55 eV at the extrapolated value to $q = 0$. In an early work [14], the extrapolation of the measured data to $q = 0$ gives plasmon linewidths somewhat smaller than 4 eV (hexagonal plane) and 3 eV (c-axis). Furthermore, a monotonically increasing half-width for $\mathbf{q}$ along the c-axis was observed. The lack of agreement between those findings and the present results can be attributed to the experimental shortcomings of early measurements, as mentioned in the introduction. Additionally, the plasmon excitation was not investigated in that work at sufficiently long wavelengths, as has been done in the present study.

It is well known that the RPA treatment of the jellium model predicts an infinitely sharp plasmon peak for $q < q_c$ and a strongly broadened one for $q > q_c$ due to the possibility of plasmon decay via electron–hole pair excitations (Landau damping). In a correlated electron system, a plasmon can decay by exciting two (or more) particle–hole pairs, giving rise to a quadratically dispersing half-width in the long-wavelength limit and vanishing at $q = 0$ [44–46]. Other possible multiple excitations (plasmon-pair and plasmon–plasmon excitations) have been discussed more recently by Sturm and Gusarov [47], but the magnitude of their contribution should be of less importance or directly vanish (plasmon–plasmon excitation) in the energy-loss range that we have investigated. For the electron density of Be, the theoretical prediction [46] gives a half-width of ∼0.25 eV at $q = 0.61$ au (the highest measured q-value). This width is about 32 times smaller than our measured value, thus indicating that dynamical electron correlations in Be have a negligible effect on the linewidth dispersion at $q < q_c$. The observed half-width at $q = 0$ is relatively large compared to that of other simple metals (tenths of an eV for Al and the alkali metals, except for Li, for which it is 2.2 eV) [9, 19, 40]. In the nearly-free-electron approximation the decay of a plasmon via interband transitions can be viewed as umklapp processes in which a reciprocal lattice vector couples the plasmon to the particle–hole pair excitation channel of the free electron gas [24]. Therefore, at $q = 0$ only those $\mathbf{G}$ vectors for which the point $(|\mathbf{G}|, \omega(0))$ falls into the excitation continuum give a non-zero contribution to the plasmon halfwidth. It can be seen that four sets of reciprocal lattice vectors (namely $\{\mathbf{G}_{100}\}$, $\{\mathbf{G}_{002}\}$, $\{\mathbf{G}_{101}\}$ and $\{\mathbf{G}_{102}\}$) contribute for Be, whereas for Al there are three [24] and for the alkali metals only one [25, 48]. In addition, the probability of such transitions for a given $\mathbf{G}$ is proportional to the square of the corresponding Fourier coefficient of the pseudo-potential [24]. Since for Be the pseudo-potential is considerably stronger compared to that of Al and the alkali metals, interband-transition-induced damping mechanisms are expected to play a much more important role in Be than in those simple metals. Further damping mechanisms have been proposed and evaluated in the literature. Plasmon decay via phonon-assisted intra- and interband transitions should be of minor importance in simple metals [24]. As pointed out by Sturm [41], the imaginary part of the core dielectric function provides a new damping mechanism, but its effect should be very small if the core excitation energies are much larger than the plasmon energy [24]. On the other hand, by performing calculations of the response function in the presence and in the absence of the contribution from higher-lying core states in K, Ku and Eguiluz [26] found that the plasmon linewidth is markedly affected by the availability of core excitations. Specifically, they observed a reduction in the linewidth when core electrons are considered. Core excitation effects could be partially responsible for the differences observed in Be, since core electrons are not included in the present calculations. Nevertheless, despite some small discrepancies between the present calculated and measured data, one can clearly conclude that, among the several possible damping mechanisms, in the case of Be, interband transitions give the leading contribution to the plasmon half-width and to its q-dependence, as is also observed in Al [24], Li [25] and K [26].

5. Conclusions

An experimental and theoretical study of the plasmon excitation in Be has been presented. Overall good agreement between the measured plasmon energy dispersion and the results from *ab initio* calculations within the RPA was found. Band-structure effects are responsible for this agreement, principally as q approaches the excitation continuum. The observed finite plasmon lifetime at $q = 0$ and the width dispersion are in fairly good agreement with present calculations. Interband transitions were found to be the main damping mechanism in Be for momentum transfers lower than the plasmon cutoff wavevector. Further measurements in single crystals are necessary to confirm the anisotropies predicted by the theory both in the plasmon energy and in the width dispersion. Theoretical studies accounting for core polarization and exchange and correlation effects could help to sort out the small remaining discrepancies.

Acknowledgments

The research was partially supported by LNLS (National Synchrotron Light Laboratory). Financial support from SeCyT (Universidad Nacional de Córdoba) and PRONEX/CNPq is gratefully acknowledged. VMS and EVC acknowledge partial support from the University of the Basque Country, the Departamento de Educación del Gobierno Vasco, and the Spanish Ministerio de Ciencia y Tecnología (MCyT) (grant no. FIS 2004-06490-C03-01), and the European Community 6th Network of Excellence NANOQUANTA (NMP4-CT-2004-500198).

References

[1] Schülke W 2001 *J. Phys.: Condens. Matter* **13** 7557
[2] Isaacs E D, Platzman P M, Zschack P, Hamalainen K and Kortan A R 1992 *Phys. Rev.* B **46** 12910
[3] Hill J P, Kao C-C, Caliebe W A C, Gibbs D and Hastings J B 1996 *Phys. Rev. Lett.* **77** 3665
[4] Sternemann C, Kaprolat A and Schülke W 1998 *Phys. Rev.* B **57** 622
[5] Burns C A, Abbamonte P, Isaacs E D and Platzman P M 1999 *Phys. Rev. Lett.* **83** 2390
[6] Hayashi H, Udagawa Y, Kao C-C, Rueff J P and Sette F 2001 *J. Electron Spectrosc. Relat. Phenom.* **120** 113
[7] Burns C A, Giura P, Said A, Shukla A, Vanko G, Tuel-Benckendorf M, Isaacs E D and Platzman P M 2002 *Phys. Rev. Lett.* **89** 236404
[8] Galambosi S, Soininen J A, Mattila A, Huotari S, Manninen S, Vankó Gy, Zhigadlo N D, Karpinski J and Hämäläinen K 2005 *Phys. Rev.* B **71** 60504
[9] Raether H 1980 *Excitations of Plasmons and Interband Transitions by Electrons* (Berlin: Springer)
[10] Pines D 1964 *Elementary Excitations in Solids* (New York: Benjamin)
[11] Priftis G 1970 *Phys. Rev.* B **2** 54
[12] Tanokura A, Hirota N and Suzuki T 1970 *J. Phys. Soc. Japan* **28** 1382
Suzuki T and Tanokura A 1970 *J. Phys. Soc. Japan* **29** 972
[13] Miliotis D M 1971 *Phys. Rev.* B **3** 701
[14] Eisenberger P, Platzman P M and Pandy K C 1973 *Phys. Rev. Lett.* **31** 311
[15] Schülke W, Nagasawa H, Mourikis S and Kaprolat A 1989 *Phys. Rev.* B **40** 12215
[16] Ichimaru S 1982 *Rev. Mod. Phys.* **54** 1017
[17] Singwi K S and Tosi M P 1981 *Correlations in Electron Liquids* (*Solid State Physics* vol 36) ed H Ehrenreich *et al* (New York: Academic) p 177
[18] Sprösser-Prou J, vom Felde A and Fink J 1989 *Phys. Rev.* B **40** 5799
[19] vom Felde A, Sprösser-Prou J and Fink J 1989 *Phys. Rev.* B **40** 10181
[20] Dabrowski B 1986 *Phys. Rev.* B **34** 4989
[21] Quong A A and Eguiluz A G 1993 *Phys. Rev. Lett.* **70** 3955
[22] Maddocks N E, Godby R W and Needs R J 1994 *Phys. Rev.* B **49** 8502
[23] Silkin V M, Chulkov E V and Echenique P M 2003 *Phys. Rev.* B **68** 205106
[24] Sturm K 1982 *Adv. Phys.* **31** 1
[25] Karlsson K and Aryasetiawan F 1995 *Phys. Rev.* B **52** 4823

[26] Ku W and Eguiluz A G 1999 *Phys. Rev. Lett.* **82** 2350
[27] Keast V J 2005 *J. Electron Spectrosc. Relat. Phenom.* **143** 97
[28] Runge E and Gross E K U 1984 *Phys. Rev. Lett.* **52** 997
[29] Petersilka M, Gossmann U J and Gross E K U 1996 *Phys. Rev. Lett.* **76** 1212
[30] Aryasetiawan F and Gunnarsson O 1994 *Phys. Rev.* B **49** 16214
[31] Aryasetiawan F 2001 *Strong Coulomb Correlations in Electronic Structure Calculations* ed V I Anisimov (Singapore: Gordon and Breach)
[32] Amonenko V M, Ivanov V Y, Tikhinskii G F and Finkel A 1962 *Fiz. Met. Metalloved.* **14** 852
Amonenko V M, Ivanov V Y, Tikhinskii G F and Finkel A 1962 *Phys. Met. Metallogr.* **14** 47 (Engl. Transl.)
[33] Ceperly D M and Alder B J 1980 *Phys. Rev. Lett.* **45** 566
as parametrized by Perdew J P and Zunger A 1981 *Phys. Rev.* B **23** 5048
[34] Silkin V M, Chulkov E V, Sklyadneva I Yu and Panin V E 1984 *Izv. Vyssh. Uchebn. Zaved. Fiz.* **9** 56
Silkin V M, Chulkov E V, Sklyadneva I Yu and Panin V E 1984 *Russ. Phys. J.* **27** 762 (Engl. Transl.)
[35] Chulkov E V, Silkin V M and Shirykalov E N 1987 *Fiz. Met. Metalloved.* **64** 213
Chulkov E V, Silkin V M and Shirykalov E N 1987 *Phys. Met. Metallogr.* **64** 1 (Engl. Transl.)
[36] Tirao G, Stutz G and Cusatis C 2004 *J. Synchrotron Radiat.* **11** 335
[37] Schülke W, Nagasawa H and Mourikis S 1984 *Phys. Rev. Lett.* **52** 2065
[38] Felsteiner J and Schülke W 1997 *Nucl. Instrum. Methods* B **132** 1
[39] Diekmann W, Eickmans J and Otto A 1986 *Z. Phys.* B **65** 39
[40] Egerton R F 1986 *Electron Energy-Loss Spectroscopy in the Electron Microscope* (New York: Plenum)
[41] Sturm K 1983 *Solid State Commun.* **48** 29
[42] Taut M 1986 *J. Phys. C: Solid State Phys.* **19** 6009
[43] Dalgarno A 1962 *Adv. Phys.* **11** 281
[44] DuBois D F and Kivelson M G 1969 *Phys. Rev.* **186** 409
[45] Hasegawa M and Watabe M 1969 *J. Phys. Soc. Japan* **27** 1393
[46] Bachlechner M, Böhm H and Schinner A 1993 *Physica* B **183** 293
[47] Sturm K and Gusarov A 2000 *Phys. Rev.* B **62** 16474
[48] Sturm K and Oliveira L E 1981 *Phys. Rev.* B **24** 3054